Original Article

Yonsei Med J 2024 Aug;65(8):434-447
https://doi.org/10.3349/ymj.2023.0308

Yonsei Medical Journal
YMJ
pISSN: 0513-5796 · eISSN: 1976-2437

Diverging Relationships among Amyloid, Tau, and Brain Atrophy in Early-Onset and Late-Onset Alzheimer's Disease

Han Kyu Na[1*], Jeong-Hyeon Shin[2*], Sung-Woo Kim[3], Seongho Seo[4,5], Woo-Ram Kim[4], Jae Myeong Kang[6], Sang-Yoon Lee[7], Jaelim Cho[8], Justin Byun[9], Nobuyuki Okamura[10], Joon-Kyung Seong[3,11], and Young Noh[4,12]

[1]Department of Neurology, Yonsei University College of Medicine, Seoul, Korea;
[2]Bio Medical Research Center, Bio Medical & Health Division, Korea Testing Laboratory, Daegu, Korea;
[3]School of Biomedical Engineering, Korea University, Seoul, Korea;
[4]Neuroscience Research Institute, Gachon University, Incheon, Korea;
[5]Department of Electronic Engineering, Pai Chai University, Daejeon, Korea;
[6]Department of Psychiatry, Gachon University Gil Medical Center, Incheon, Korea;
[7]Department of Neuroscience, College of Medicine, Gachon University, Incheon, Korea;
[8]Department of Preventive Medicine, Yonsei University College of Medicine, Seoul, Korea;
[9]Department of Rehabilitation Medicine, Severance Hospital, Yonsei University College of Medicine, Seoul, Korea;
[10]Division of Pharmacology, Faculty of Medicine, Tohoku Medical and Pharmaceutical University, Sendai, Japan;
[11]Department of Artificial Intelligence, Korea University, Seoul, Korea;
[12]Department of Neurology, Gil Medical Center, Gachon University College of Medicine, Incheon, Korea.

Purpose: Alzheimer's disease (AD) dementia may not be a single disease entity. Early-onset AD (EOAD) and late-onset AD (LOAD) have been united under the same eponym of AD until now, but disentangling the heterogeneity according to the age of sonset has been a major tenet in the field of AD research.

Materials and Methods: Ninety-nine patients with AD (EOAD, n=54; LOAD, n=45) and 66 cognitively normal controls completed both [^{18}F]THK5351 and [^{18}F]flutemetamol (FLUTE) positron emission tomography scans along with structural magnetic resonance imaging and detailed neuropsychological tests.

Results: EOAD patients had higher THK retention in the precuneus, parietal, and frontal lobe, while LOAD patients had higher THK retention in the medial temporal lobe. Intravoxel correlation analyses revealed that EOAD presented narrower territory of local FLUTE-THK correlation, while LOAD presented broader territory of correlation extending to overall parieto-occipito-temporal regions. EOAD patients had broader brain areas which showed significant negative correlations between cortical thickness and THK retention, whereas in LOAD, only limited brain areas showed significant correlation with THK retention. In EOAD, most of the cognitive test results were correlated with THK retention. However, a few cognitive test results were correlated with THK retention in LOAD.

Conclusion: LOAD seemed to show gradual increase in tau and amyloid, and those two pathologies have association to each other. On the other hand, in EOAD, tau and amyloid may develop more abruptly and independently. These findings suggest LOAD and EOAD may have different courses of pathomechanism.

Key Words: Early-onset Alzheimer's disease, late-onset Alzheimer's disease, positron emission tomography, tau, amyloid, cortical thickness

Received: July 27, 2023 **Revised:** January 20, 2024 **Accepted:** January 23, 2024 **Published online:** June 12, 2024
Co-corresponding authors: Young Noh, MD, PhD, Department of Neurology, Gil Medical Center, Gachon University College of Medicine, 21 774-gil, Namdong-daero, Namdong-gu, Incheon 21565, Korea.
E-mail: ynoh@gilhospital.com and
Joon-Kyung Seong, PhD, School of Biomedical Engineering, Korea University, 145 Anam-ro, Seongbuk-gu, Seoul 02841, Korea.
E-mail: jkseong@korea.ac.kr

*Han Kyu Na and Jeong-Hyeon Shin contributed equally to this work.
•The authors have no potential conflicts of interest to disclose.

INTRODUCTION

As there has been mounting evidence supporting that Alzheimer's disease (AD) dementia may not be a single disease entity, disentangling the heterogeneity of AD has been a major tenet in the field of AD research for decades.[1,2] Among the various factors affecting the variable course of AD, the age of onset is widely accepted as one of the most important determinants of this AD heterogeneity. Although AD occurs mostly in the elderly [age ≥65 years, late-onset AD (LOAD)], a certain proportion of AD patients show onset of symptoms before the age of 65, namely the early-onset AD (EOAD). Until now, EOAD and LOAD have been united under the same eponym based on the fact that they share core neuropathological hallmarks in common. However, numerous research groups continue to report marked differences between EOAD and LOAD in terms of cognitive profile, prognosis, and topographic distribution of neuropathological burden.[1-5]

With the advent of tau-targeted positron emission tomography (PET) tracers,[6-8] in vivo visualization of neurofibrillary tangle (NFTs) has become possible, thereby allowing us to investigate the tau pathology even in earlier stage of AD. Recent studies have reported that tau signal correlates closely with cerebral atrophy, cognitive deficit, and also show highly consistent finding with post-mortem histopathology.[7,8] Together, these findings suggest that PET studies using the tau-targeted tracers may provide us with a better understanding for the pathomechanism underlying AD.

Accumulating evidence suggest that amyloid and tau do not necessarily follow the temporal order, and that they sometimes exert their effect independently to induce neurodegeneration.[9,10] In addition to temporal perspective, the spatial discordance among amyloid, tau, and neurodegeneration has also been observed; and the two major pathologies are known to cause downstream neurodegeneration in complex mechanism showing synergistic interaction in some regions[11] but also work independently to each other in other regions.[10] Moreover, a variety of patterns of interaction ranging from local-to-local and local-to-distributed cortical associations between amyloid and tau is now being actively reported.[9] To date, few studies have compared the differential distribution of both tau and amyloid simultaneously in AD patients according to the age of onset,[12,13] and how the amyloid-tau interaction in AD differs according to age of onset remains an area of active debate.

Concerns have been raised regarding the off-target binding of the first generation tau PET tracers.[14] Studies have indicated that [^{18}F]THK5351 binding to monoamine oxidase-B (MAO-B) significantly contributes to in vivo tau PET signal. Recent research has shown that THK family radiotracers can distinguish well between AD dementia and healthy controls, and that it may be a suitable imaging marker to detect neurodegenerative changes caused by reactive astrogliosis as well as tau.[15,16] However, it still restricts the clinical interpretation of research using this tracer by not purely reflecting only tau, but other factors as well.

The objectives of this study were to compare the overall tau topography in EOAD and LOAD and to investigate the differential pattern of interaction among amyloid, tau, and neurodegeneration according to the age of onset. As amyloid and tau pathology both serve as major hallmarks of AD, the characterization of tau pathology in conjunction with amyloid would allow us to better disentangle the AD heterogeneity according to the age of onset, a conundrum that has remained unsolved for decades.

MATERIALS AND METHODS

Participants

One hundred sixty-seven participants who had been clinically diagnosed with EOAD dementia (n=54) and LOAD dementia (n=47), and 66 cognitively normal (CN) subjects were prospectively recruited from October 2015 to September 2017. All participants underwent 3.0-Tesla MRI, ^{18}F-THK5351 PET scans, and [^{18}F]flutemetamol (FLUTE) PET scans, and completed neuropsychological test at Memory Clinic at Gachon University Gil Medical Center. Out of 167 participants, two patients with LOAD were excluded for head motion during [^{18}F]THK5351 PET scan acquisition. Finally, a total of 165 participants were included in this study.

All patients with AD dementia had been diagnosed with probable AD according to the National Institute of Neurological and Communicative Disorders and Stroke and the AD and Related Disorders Association, and the diagnoses were confirmed by follow-up for more than 1 year at the outpatient clinics. EOAD was defined as AD patients whose onset age was under 65 years, and LOAD as AD patients whose onset age was over 65 years. Patients with other structural lesions on brain MRI, such as territorial infarction, intracranial hemorrhage, traumatic brain injury, hydrocephalus, severe white matter hyperintensity (WMH) or WMH associated with radiation, multiple sclerosis, or vasculitis, were excluded from this study. Patients with familial AD were also exlucded. All participants completed a clinical interview and underwent a standardized neuropsychological examination.

Detailed test items of neuropsychological examinations and aphasia battery are presented in Supplementary Material (only online). Secondary causes of dementia were ruled out through laboratory tests assessing complete blood counts, vitamin B_{12}, folate levels, thyroid function, metabolic profile, and syphilis serology. APOE genotyping was also performed.

The CN subjects were recruited from volunteers in the community or spouses of patients at the Memory Disorder Clinic of Gil Medical Center. All CN subjects had no history of neurological/psychiatric illnesses or abnormalities detected on neurologic examination. The subjects were required to have a clinical dementia rating (CDR) of 0, and normal cognitive func-

tion defined as within 1.5 standard deviations of the age- and education-corrected normative mean as determined by neuropsychological tests. There were no structural lesions, including cerebral infarction, intracranial hemorrhage, traumatic brain injury, hydrocephalus, or severe WMH, detected in brain MRI scans of the CN subjects. For comparison with the EOAD or LOAD groups, CN subjects were divided into age-matched control groups, each comprising 33 young controls (YC) (mean age: 57.6 years) and 33 old controls (OC) (mean age: 75.7 years).

Written informed consent was obtained from all participants, and the study was approved by the Institutional Review Board of Gachon University Gil Medical Center (IRB No. GDIRB2015-272).

Image acquisition and preprocessing

MR image acquisition and parcellation

The study participants underwent brain MR imaging using Verio 3.0-Tesla MRI scanner (Siemens, Erlangen, Germany) to acquire 3D T1-MPRAGE. The images were analyzed using FreeSurfer 6.0 (Massachusetts General Hospital, Harvard Medical School; http://surfer.nmr.mgh. harvard.edu) to define the regions-of-interest (ROIs) in the native space of each participant and to support a correction of gray matter (GM) atrophy and white matter spillover in the PET data. Other clinical MRI sequences, including the fluid attenuated inversion recovery (FLAIR), susceptibility weighted imaging (SWI), and T1- and T2-weighted imaging, were also acquired. The FLAIR imaging parameters used were as follows: repetition time=9000 ms, echo time=122 ms, flip angle=150°, pixel bandwidth=287 Hz/pixel, matrix size=256×224. The SWI imaging parameters used were as follows: repetition time=27 ms, echo time=20 ms, flip angle=15°, pixel bandwidth=120 Hz/pixel, matrix size=256×224. T1-weighted imaging parameters used were as follows: repetition time=500 ms, echo time=9.2 ms, flip angle=70°, pixel bandwidth=391 Hz/pixel, matrix size=256×224. T2-weighted imaging parameters used were as follows: repetition time=9650 ms, echo time=88 ms, flip angle=120°, pixel bandwidth=174 Hz/pixel, matrix size=256×224.

Surface-based cortical thickness (CTh) was calculated using FreeSurfer. We first constructed the outer and inner cortical surface meshes from the MR volume of each subject. The two meshes were isomorphic with the same vertices and connectivity, as the outer surface was constructed by deforming the inner surface. In order to establish correspondence between subjects, we resampled each subject's cortical surface to 40962 vertices for each hemisphere using the previously proposed method.[17] The vertex-wise CTh at each vertex was defined as the distance between the two surfaces at the vertex.

Lacunes were defined as lesions of ≥3 mm and ≤15 mm in diameter with low signal on T1-weighted images, high signal on T2-weighted images, and a perilesional halo on 80 axial sections of FLAIR images. Microbleeds were defined as small lesions of ≤10 mm in diameter on 20 axial sections of time constant for T2-weighted gradient–recalled echo sequence MRIs. Images were analyzed using FreeSurfer 6.0.

PET image acquisition

All PET scans were acquired with a Siemens Biograph 6 Truepoint PET/computed tomography (CT) scanner (Siemens) with a list-mode emission acquisition. [^{18}F]THK5351 was synthesized and radiolabeled at Gachon University Neuroscience Research Institute. All participants underwent a 20-minute emission scan starting 50 minutes after 185 MBq of [^{18}F]THK5351 was injected intravenously (50–70 minutes) and a 20-minute emission scan starting 90 minutes after the intravenous injection of 185 MBq of [^{18}F]FLUTE (90–110 minutes), which was purchased from Carecamp Inc. and radiolabeled at the Gachon University Neuroscience Research Institute. A low-dose CT was performed for attenuation correction prior to all scans. In participants who underwent [^{18}F]THK5351 and [^{18}F]FLUTE PET scans, the mean intervals between THK PET and FLUTE PET scans were 10 days. FLUTE PET and MRI scans were acquired on the same day. Individual static images were reconstructed onto a 256×256×109 matrix with a voxel size of 1.3×1.3×1.5 mm^3 using a 2D ordered subset expectation maximization algorithm (8 iterations and 16 subsets), with corrections for physical effects.

PET quantification

Each [^{18}F]THK5351 or [^{18}F]FLUTE PET image was co-registered with the corresponding T1 image using FreeSurfer and smoothed with an 8-mm Gaussian kernel. Regional mean values of PET images were then extracted after region-based partial volume correction (PVC) using the PETSurfer tool in FreeSurfer[18,19] and the resultant weighted-average for pre-defined ROIs. ROIs included the frontal cortex (caudal middle frontal, lateral orbitofrontal, medial orbitofrontal, pars opercularis, pars orbitalis, pars triangularis, precentral, rostral middle frontal, superior frontal cortices, and frontal pole), lateral temporal cortex (banks of superior temporal sulcus, inferior temporal, middle temporal, and superior temporal cortices), superior parietal cortex (post central and superior parietal), inferior parietal cortex (inferior parietal and supramarginal gyrus), occipital cortex (cuneus, pericalcarine, and lateral occipital cortices), anterior cingulate cortex (accumbens and caudal anterior cingulate cortex), precuneus and posterior cingulate cortex (PCC), mesial temporal (hippocampus, parahippocampal gyrus, amygdala, and entorhinal cortex), hippocampus, entorhinal cortex, fusiform gyrus, lingual gyrus, basal ganglia (caudate, putamen and pallidum), and global cortex (a composition of the frontal, lateral temporal, superior parietal, inferior parietal, occipital, anterior cingulate cortex, precuneus-PCC, mesial temporal, fusiform gyrus, and lingual gyrus). Regional standardized uptake value ratios (SUVRs) were calculated using cerebellar GM as the reference region for THK images and the pons for FDG and FLUTE images.[20] SUVR images were also

https://doi.org/10.3349/ymj.2023.0308

generated from the MRI co-registered PET images with voxel-based PVC.[18,19] Cortical retention ratio of FLUTE was calculated based on AD-related regions, including the frontal, parietal, lateral temporal, anterior, and posterior cingulate cortices.[20] Amyloid positivity with FLUTE images were evaluated visually in the frontal, temporal, parietal cortices, striatum, and precuneus.

Statistical analyses

Comparisons of demographic and clinical data between diagnostic groups were conducted using one-way analysis of variance with Bonferroni correction (p<0.05). Categorical variables were evaluated using the chi-square test. Regional THK SUVRs, as well as FLUTE SUVRs, were compared between the three groups using a one-way analysis of covariance with adjustment for age and years of education, and pairwise differences among the adjusted means were further evaluated with Bonferroni correction (p<0.05). Correlations between the neuropsychological data and regional THK SUVR were evaluated with Pearson correlation analysis. Region-wise multiple comparisons were corrected in analyses of ROIs by using the Benjamini-Hochberg false discovery rate method. In order to examine the left and right regional correlation between THK SUVR and each cognitive function, multiple linear regression analysis was performed using cognitive function as the independent factor and the regional THK5351 SUVR as the dependent variable after adjusting for THK5351 SUVR in the global neocortex. Sensitivity analysis was performed. To examine the interaction effect of onset age as a continuous variable, we conducted the analysis without dividing between AD patients in terms of EOAD and LOAD. We set the product of onset age and regional THK5351 SUVR as an interaction term, adjusting for onset age, sex, education years, and disease duration, and evaluated the relationship between regional THK and regional FLUTE using general linear model. All the statistical analyses mentioned above were conducted with the PASW Statistics 23 software (SPSS Inc, Chicago, IL, USA) with a significance of p<0.05 (two-tailed).

SPM multiple regression analyses

We analyzed multiple regression analyses of THK5351 retention to find correlation with global FLUTE retention, and to find correlation with mean CTh using Statistical Parametric Mapping 5 (SPM5). The analyses were performed with adjustments for age, sex, and educational years. The results were presented as p<0.001, uncorrected for multiple comparisons.

BPM analysis preprocessing and statistics

To evaluate the intra-voxel correlation between [^{18}F]THK5351 retention and [^{18}F]FLUTE retention in each diagnostic group, voxel-wise partial correlation analyses between the two tracers were performed with adjustment for age. Biological Parametric Mapping (BPM) 3.1 toolbox with SPM5 was used. Any predefined brain mask was not applied, and the absolute p value threshold was used. The resulting t-score maps (uncorrected p<0.01, cluster>100) for partial correlation were overlaid on an inflated FSaverage brain.

Correlation analysis between image markers (correlation matrices)

To investigate inter-regional correlations of THK retention and FLUTE retention or regional CTh, correlation matrices were calculated from partial correlation analysis with adjustment of age. We performed correlation analysis between regional THK5351 retention and FLUTE retention in 88 ROIs. We also performed correlation analysis between image markers computed from T1-weighted MR images and PET images of 70 ROIs, which included 68 cortical regions in both hemispheres and both hippocampi. Image markers computed from MR images included CThs and volumes for cortical regions and hippocampi, respectively. Image markers computed from PET images were ROI-averaged SUVR for all 70 ROIs. We computed Spearman's rho after controlling for the effects of age, sex, and education year. For clarification, Spearman's rho value passing threshold p value<0.01 was also presented.

Surface-based correlation analyses between CTh and global THK retention

We performed the correlation analysis between 81924 vertices for vertex-wise CTh and global THK retention using the Spearman partial correlation adjusted for age, sex, and educational years. For multiple comparison correction, we employed Cluster-based statistics (CBS). CBS estimated significance levels of cluster based on how the cluster size was bigger than the randomly formed cluster using permutation testing, where a cluster was defined as a set of connected vertices has correlation coefficient above absolute 0.3. Specifically, we re-populated global THK retention of the data sets N-1 times by random permutation, where N is the number of permutations. We computed the maximum size of clusters for the original data set and N-1 permuted sets, which resulted in a null distribution of sizes of the randomly formed clusters. Then, we estimated the significance level by a fraction of the occurrence whose sizes of the randomly formed clusters were no less than the original cluster size. We used 5000 as N.

RESULTS

Demographic and clinical characteristics

Detailed information regarding demographic and clinical characteristics of EOAD, LOAD, and their age-matched controls are summarized in Table 1. The age of onset was much younger in EOAD (56.69±5.27) compared to LOAD (73.40±6.03) (p<0.001), and the length of education years was longer in EOAD (9.47±3.91 vs. 7.50±5.17, p=0.038). The proportion of patients with APOE ε4 allele did not differ significantly between EOAD and

Table 1. Demographics and Clinical Characteristics of the Study Population

Variables	EOAD (n=54)	YC (n=33)	EOAD vs. YC *p* value	LOAD (n=45)	OC (n=33)	LOAD vs. OC *p* value	EOAD vs. LOAD *p* value
Age (yr)	60.46±5.40	57.55±7.17	0.049*	77.89±6.31	75.46±5.40	0.078	<0.001*
Age at onset (yr)	56.69±5.27	-		73.40±6.03	-		<0.001*
Sex (female)	37 (68.5)	13 (39.4)	0.008*	33 (73.3)	18 (54.5)	0.085	0.600
Education (yr)	9.47±3.91	13.46±3.52	<0.001*	7.50±5.17	10.58±5.24	0.012*	0.038*
Disease duration (month)	42.93±20.36	-		53.89±31.65	-		0.049*
MMSE	17.34±5.60	28.76±1.15	<0.001*	18.21±6.06	27.09±2.47	<0.001*	0.474
CDR SOB	5.63±3.86	0.00±0.00	<0.001*	5.23±3.25	0.00±0.00	<0.001*	0.586
APOE ε4 (carrier)	25 (46.3)	8 (24.2)	0.040*	24 (53.3)	6 (18.2)	0.002*	0.486
Amyloid positivity	54 (100)	0 (0.0)	<0.001*	43 (95.6)	2 (6.1)	<0.001*	0.226
Hypertension	10 (18.5)	7 (21.2)	0.759	20 (44.4)	18 (54.5)	0.378	0.005*
Diabetes mellitus	9 (16.7)	3 (9.1)	0.320	5 (11.1)	6 (18.2)	0.375	0.430
Coronary artery disease	1 (1.9)	0 (0.0)	0.432	6 (13.3)	5 (15.2)	0.820	0.026*
Dyslipidemia	9 (16.7)	13 (39.4)	0.018*	17 (37.8)	13 (39.4)	0.885	0.017*
History of stroke	1 (1.9)	0 (0.0)	0.432	2 (4.4)	1 (3.0)	0.748	0.454
Total lacune	0.66±0.98	0.48±0.80	0.389	1.56±2.30	0.91±1.23	0.147	0.018*
Total microbleeds	0.08±0.27	0.09±0.38	0.827	0.71±2.57	0.06±0.24	0.099	0.106
Total WMH volume (mm^3)	4539.46±3895.98	2431.91±1685.94	0.001*	7612.93±6568.54	5158.39±5341.67	0.082	0.007*
PWMH	4165.57±3533.66	2158.52±1554.85	<0.001*	6955.16±5754.29	4505.45±4105.23	0.040*	0.006*
DWMH	373.89±666.20	273.37±337.42	0.423	657.78±1076.57	652.94±1401.70	0.986	0.128
Mean CTh (mm)	2.29±0.16	2.49±0.08	<0.001*	2.34±0.12	2.45±0.09	<0.001*	0.066
Hippocampal volume (mm^3)	3116.85±473.39	4418.79±301.85	<0.001*	2850.24±454.01	3800.88±316.43	<0.001*	0.005*
ICV (mm^3)	1369857.26±195320.74	1367074.02±175510.72	0.947	1403582.69±156825.79	1430956.37±173270.96	0.469	0.353

EOAD, early-onset Alzheimer's disease; YC, young control; LOAD, late-onset Alzheimer's disease; OC, old control; MMSE, Mini-Mental State Examination; CDR–SOB, clinical dementia rating–sum of boxes; WMH, white matter hyperintensity; PWMH, periventricular white matter hyperintensity; DWMH, deep white matter hyperintensity; CTh, cortical thickness; ICV, intracranial volume.
Data are presented as mean±standard deviation for continuous variables and number (%) for nominal variables. Independent t-test was performed for continuous variables and chi-square test for nominal variables.
*Significant (p<0.05).

LOAD groups (p=0.486). LOAD group showed higher proportion of patients with underlying vascular risk factors: hypertension (p=0.005), dyslipidemia (p=0.017), and coronary artery disease (p=0.026). Along with this, patients with LOAD exhibited higher burden of vascular markers compared to their younger counterpart, as revealed by the higher number of lacune (p=0.018) and volume of WMH (p=0.007). While the hippocampal volume was significantly smaller in LOAD (p=0.005), the mean CTh tended to be thinner in EOAD, though the difference failed to reach statistical significance (p=0.066).

Compared to their age-matched controls, EOAD and LOAD showed worse performance in every item of the neuropsychological battery. In direct comparison between EOAD and LOAD, EOAD exhibited worse performance in the attention, visuospatial, memory, and frontal executive function domain, leaving the language domain to be the only exception. The detailed results of neuropsychological tests are presented in Supplementary Table 1 (only online).

Difference in [^{18}F]THK5351 uptake patterns between EOAD and LOAD

Voxel-wise analyses between AD and each age-matched controls showed that nearly all association cortices were involved in EOAD. The differences between LOAD and OC seemed to be lesser than those between EOAD and YC (Supplementary Fig. 1, only online). Direct comparison between EOAD and LOAD showed that EOAD had more THK retention in the bilateral precuneus, dorsolateral prefrontal, and inferior parietal areas. Meanwhile, LOAD had greater THK retention in the brain areas around the basal forebrain and the lateral temporal areas (Fig. 1).

ROI-based analyses revealed that global cortical [^{18}F]THK5351 retention did not show significant difference between EOAD and LOAD (Table 2). In the comparison of regional [^{18}F]THK5351 SUVR, the regions showing preferential [^{18}F]THK5351 binding were distinct according to the age of onset. Compared to LOAD, EOAD showed higher [^{18}F]THK5351 SUVR in the precuneus, anterior and posterior cingulate, and posterior parietal regions (superior and inferior parietal lobule). In contrast, LOAD showed higher [^{18}F]THK5351 retention in the entorhinal (p=

https://doi.org/10.3349/ymj.2023.0308

0.004), parahippocampal (p=0.061), and along the orbito-amygdalo-hippocampal axis [orbitofrontal (p=0.065), amygdala (p=0.035), and hippocampus (p=0.014)]. Detailed information regarding [^{18}F]THK5351 retentions in AD patients and controls are presented in Table 2.

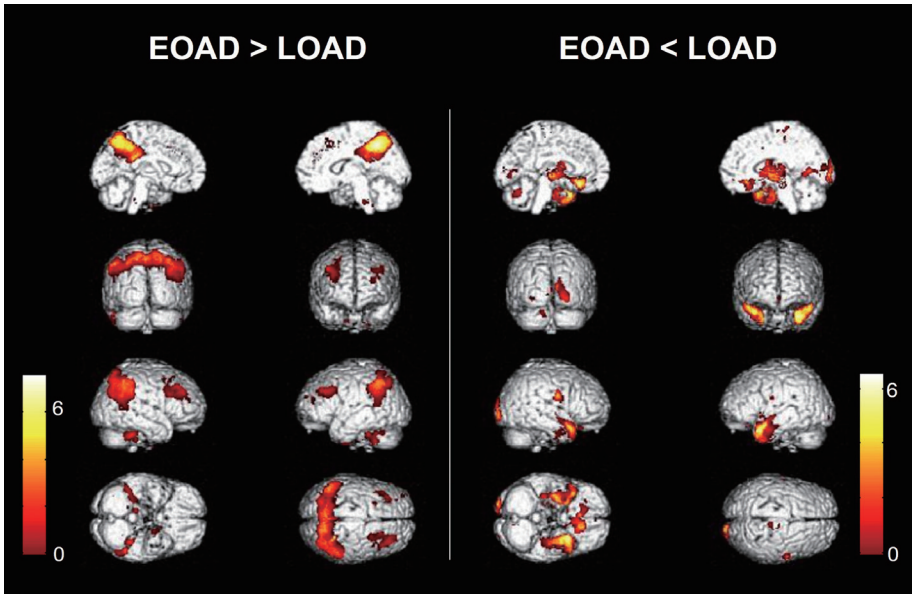

Fig. 1. Comparison of [^{18}F]THK5351 retention between EOAD and LOAD. Differences between EOAD and LOAD are presented after adjusting for age, sex, and educational years at uncorrected p value<0.001. EOAD, early-onset Alzheimer's disease; LOAD, late-onset Alzheimer's disease.

Table 2. Regional SUVR of [^{18}F] THK5351 PET

ROIs	EOAD (n=54)	YC (n=33)	EOAD vs. YC *p* value	LOAD (n=45)	OC (n=33)	LOAD vs. OC *p* value	EOAD vs. LOAD *p* value
Prefrontal	2.16±0.48	1.38±0.20	<0.001*	2.05±0.34	1.69±0.24	<0.001*	0.243
Orbitofrontal	2.46±0.51	1.82±0.25	<0.001*	2.63±0.38	2.22±0.33	<0.001*	0.065
Sensorimotor	1.29±0.29	1.09±0.18	<0.001*	1.40±0.31	1.32±0.20	0.148	0.064
Anterior cingulate	3.23±0.46	2.95±0.45	0.005*	3.51±0.48	3.25±0.40	0.015*	0.005*
Superior parietal	2.25±0.77	1.20±0.17	<0.001*	1.84±0.46	1.44±0.21	<0.001*	0.002*
Inferior parietal	2.67±0.76	1.30±0.19	<0.001*	2.16±0.52	1.62±0.23	<0.001*	<0.001*
Precuneus	2.83±0.79	1.46±0.21	<0.001*	2.30±0.57	1.75±0.24	<0.001*	<0.001*
Posterior cingulate	2.90±0.59	1.90±0.22	<0.001*	2.66±0.51	2.20±0.37	<0.001*	0.036*†
Occipital	1.52±0.54	1.02±0.14	<0.001*	1.63±0.46	1.23±0.20	<0.001*	0.293
Superior temporal	2.11±0.43	1.61±0.21	<0.001*	2.33±0.48	1.92±0.30	<0.001*	0.014
Middle temporal	2.82±0.84	1.63±0.25	<0.001*	2.72±0.64	1.98±0.30	<0.001*	0.494
Inferior temporal	2.69±0.73	1.59±0.23	<0.001*	2.69±0.62	1.96±0.29	<0.001*	0.983
Mesial temporal	3.48±0.61	2.48±0.28	<0.001*	3.93±0.97	2.79±0.39	<0.001*	0.006*
Entorhinal	3.12±0.75	2.17±0.35	<0.001*	3.89±1.57	2.45±0.37	<0.001*	0.004*
Parahippocampus	2.61±0.60	1.93±0.30	<0.001*	2.83±0.54	2.27±0.42	<0.001*	0.061
Hippocampus	3.45±0.57	2.51±0.28	<0.001*	3.81±0.85	2.76±0.35	<0.001*	0.014*
Amygdala	5.08±1.01	3.28±0.46	<0.001*	5.76±1.91	3.73±0.60	<0.001*	0.035*†
Fusiform gyrus	2.32±0.59	1.53±0.18	<0.001*	2.44±0.63	1.83±0.26	<0.001*	0.310
Lingual gyrus	1.54±0.44	1.18±0.19	<0.001*	1.66±0.47	1.38±0.21	0.001*	0.189
Striatum	3.35±0.56	2.95±0.44	0.001*	3.93±0.69	3.60±0.53	0.025*	<0.001*
Cortical	2.37±0.45	1.48±0.19	<0.001*	2.25±0.39	1.78±0.23	<0.001*	0.165

SUVR, standardized uptake value ratio; PET, positron emission tomography; ROI, region of interest; EOAD, early-onset Alzheimer's disease; YC, young control; LOAD, late-onset Alzheimer's disease; OC, old control; FDR, false discovery rate.
Data are presented as mean±standard deviation. Adjusted for age and year of education for comparison between EOAD vs. YC and LOAD vs. OC. Adjusted for year of education for comparison between EOAD vs. LOAD.
*Significant (p<0.05); †ROIs did not survive region-wise FDR correction for multiple comparisons.

Correlation between cognitive function and regional [^{18}F]THK5351 retention

In EOAD, neuropsychological performance revealed a close link with the burden of [^{18}F]THK5351, except for Seoul Verbal Learning Test (SVLT) delayed recall. Regional THK retention, other than the anterior cingulate and occipital cortex, was correlated with cognitive functions in EOAD. However, limited items in the neurological test showed a significant correlation with a few ROIs. Visuospatial function (Rey Complex Figure Test copy) was correlated with regional THK retention in the prefrontal, superior parietal, precuneus, and occipital areas. Regional THK retention in the inferior temporal area showed correlation with Mini-Mental State Examination, clinical dementia rating-sum of boxes, Korean version of Boston Naming Test, SVLT, immediate recall, and Controlled Oral Word Association Test animal (Supplementary Tables 2 and 3, only online).

Correlation between [^{18}F]THK5351 and [^{18}F]FLUTE retention

The detailed results of correlation analyses between regional [^{18}F]THK5351 and [^{18}F]FLUTE SUVR are presented in the form of correlation matrix in Fig. 2A and B. In patients with EOAD, the regional [^{18}F]THK5351 SUVR in the inferior parietal, precuneus, superior parietal, banks of the superior temporal sulcus, cuneus, lateral occipital cortex, lingual cortex, and pericalcarine cortex was positively associated with the regional FLUTE in the same ROIs (diagonal line). Patients with LOAD

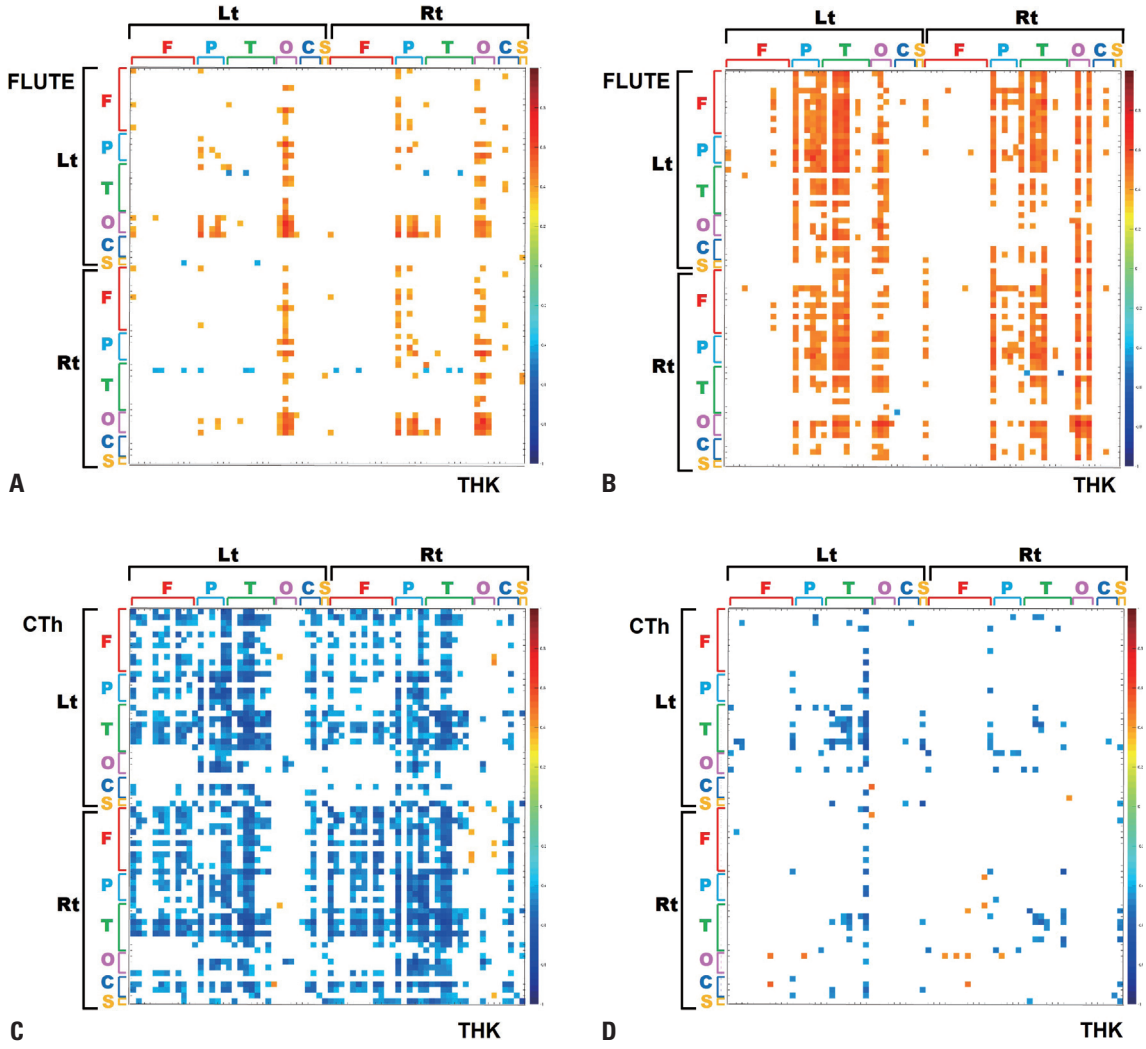

Fig. 2. Correlation matrices of the r values from partial correlations between regional THK and FLUTE or CTh. (A and B) Correlation matrices of the r values from partial correlations between 70 ROIs THK and FLUTE regional SUVRs in EOAD (A) and LOAD (B). X axis shows 70 regional SUVR of THK and Y axis presents regional SUVR of FLUTE retention (upper row). Matrices presents r values passing threshold *p* value<0.01. (C and D) Correlation matrices of the r values from partial correlations between 70 regional SUVRs of THK and 68 ROIs of CTh or hippocampal volumes. X axis shows regional SUVR of THK and Y axis presents regional CTh and hippocampal volume (upper row) in EOAD (C) and LOAD (D). Matrices presents r values passing threshold *p* value<0.01. Lt, left; Rt, right; F, frontal cortex; P, parietal cortex; T, temporal cortex; O, occipital cortex; C, cingulate cortex; S, subcortical structure; FLUTE, [^{18}F]flutemetamol; THK, [^{18}F]THK 5351; CTh, cortical thickness; ROI, regions-of-interest; SUVR, standardized uptake value ratio; EOAD, early-onset Alzheimer's disease; LOAD, late-onset Alzheimer's disease.

https://doi.org/10.3349/ymj.2023.0308

showed positive correlation between regional [^{18}F]THK5351 and [^{18}F]FLUTE SUVR in much broader territory mostly in the parieto-occipito-temporal regions as follows: middle frontal gyrus, precuneus, inferior, and superior parietal lobule (supramarginal, angular gyrus), occipital lobe (cuneus, lingual, lateral occipital cortex), fusiform, and temporal lobe (superior, middle, and inferior temporal gyrus). For better visualization, intravoxel correlation confirmed by BPM analyses are depicted in Fig. 3.

Regional [^{18}F]THK5351 SUVR was positively correlated with [^{18}F]FLUTE SUVR in distant regions in LOAD, while such associations were less observed in EOAD. The most pronounced positive correlation observed was regional [^{18}F]THK5351 SUVR in the parieto-temporal regions (precuneus, superior and inferior parietal lobule, superior and middle temporal gyrus) and [^{18}F]FLUTE SUVR throughout the neocortex. Detailed results of correlation analyses between distant regions are depicted in the form of correlation matrix (Fig. 2A). Supplementary Fig. 2A (only online) demonstrates regions of THK retention showing significantly positive correlation with global FLUTE retention. EOAD showed sparse correlation between THK and FLUTE. Meanwhile, LOAD had significantly more generalized cortical regions where THK and FLUTE had significant positive correlations (Supplementary Fig. 3, online only).

For sensitivity analysis, we combined AD patients without distinguishing between EOAD and LOAD, and examined the interaction effect of onset age in the relationship between THK and FLUTE. The results indicated that the interaction term was statistically significant in the parietal, temporal, and occipital areas (Supplementary Table 4, only online).

Correlation between THK retention and CTh

Fig. 2C and D and Fig. 4 show negative association between THK retention and CTh. In the EOAD, the thinner the cortex, the greater the THK retention in most of the neocortices. The number of cortical vertices significantly correlated with global THK SUVR was 7266 (left) and 9652 (right) in EOAD (Fig. 4). Otherwise, correlation matrix of LOAD showed there was much less regions where the regional THK SUVR and CTh were correlated significantly. The number of cortical vertices significantly correlated with global THK SUVR was 803 (left) and 0 (right) in LOAD (Fig. 4). Supplementary Fig. 2B (only online) demonstrates regions of THK retention showing significantly negative correlation with mean CTh. EOAD showed that most of association cortices correlated with mean CTh, while LOAD showed that a small number of regions correlated with CTh.

Patterns of association among amyloid, tau, and cortical atrophy

A total of six patterns of correlation among amyloid, tau, and cortical atrophy may be observed in this study. There were regions where the burden of amyloid and tau showed significant positive correlation but their relations with cortical atrophy were different: regions showing significant mutual correlation among amyloid, tau, and cortical atrophy (Fig. 5A); regions showing significant amyloid-tau correlation, but in which brain atrophy did not yet take place (Fig. 5B); and regions showing significant amyloid-tau correlation, but in which the

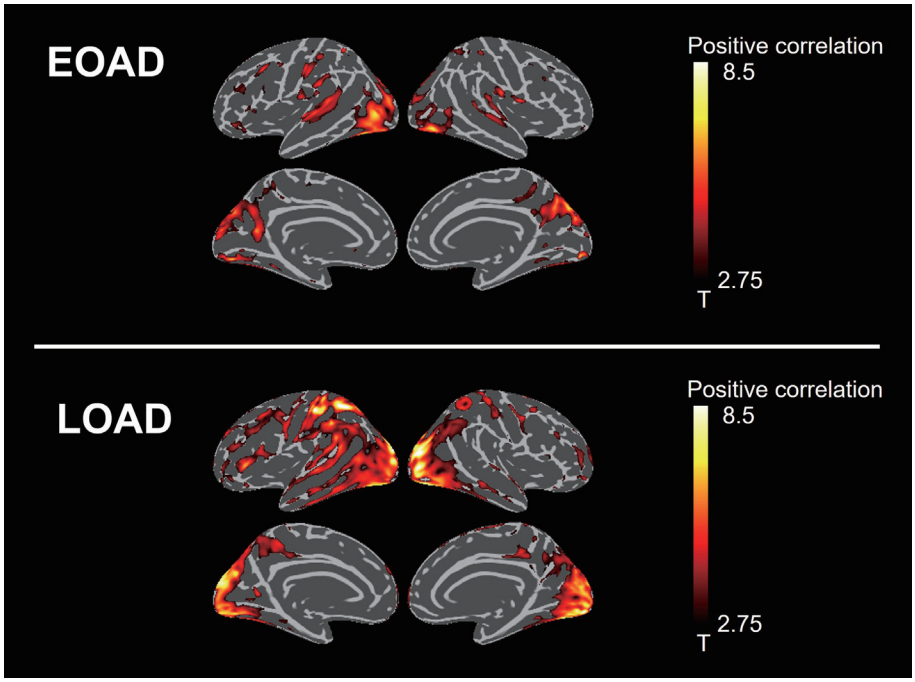

Fig. 3. Intra-voxel correlation between THK and FLUTE with BPM analysis. Intra-voxel correlation was performed after adjusting for age, sex and educational years with significance defined as an $p<0.01$ with FDR correction. FLUTE, [^{18}F]flutemetamol; THK, [^{18}F]THK 5351; BPM, biological parametric mapping; EOAD, early-onset Alzheimer's disease; LOAD, late-onset Alzheimer's disease; FDR, false discovery rate.

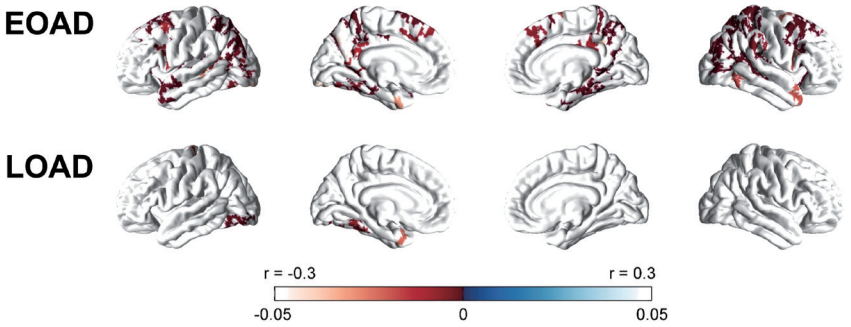

Fig. 4. Surface-based analyses of partial correlations between vertex-wise cortical thickness and global THK. Partial correlations between 81924 vertices for vertex-wise cortical thickness and global THK retention are presented after adjusting for age, sex and educational years with CBS corrected for multiple comparisons. EOAD, early-onset Alzheimer's disease; LOAD, late-onset Alzheimer's disease; CBS, Cluster-based statistics.

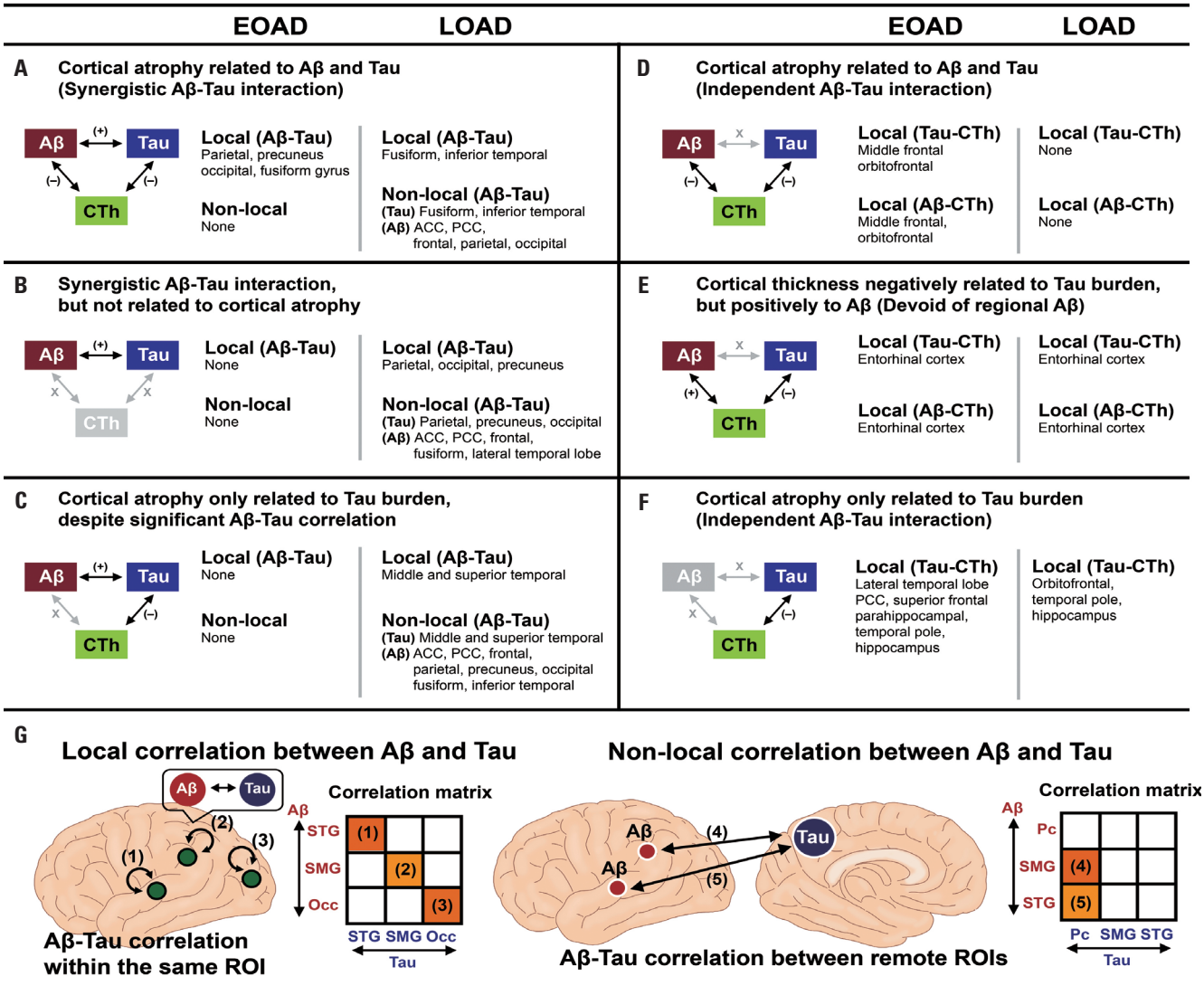

Fig. 5. Representative patterns of relationship among amyloid, tau, and cortical atrophy. (A) Regions showing significant mutual correlation among amyloid, tau, and cortical atrophy. (B) Regions showing significant amyloid-tau correlation, but in which neurodegeneration did not yet take place. (C) Regions showing significant amyloid-tau correlation, but for which the cortical atrophy only correlated to tau burden. Meanwhile, there were also regions in which amyloid and tau did not reveal any significant correlation. (D) Regions in which the CTh was negatively correlated to amyloid and tau respectively, but the two proteinopathies were independent. (E) Regions in which the CTh was negatively correlated to tau, but positively correlated to amyloid. (F) Regions in which the cortical atrophy correlated to tau only, without interaction with amyloid. (G) Schematic illustration depicting the local (within the same ROI) and non-local (between remote ROIs) correlation between amyloid, tau, and CTh. EOAD, early-onset Alzheimer's disease; LOAD, late-onset Alzheimer's disease; CTh, cortical thickness; ROI, regions-of-interest; ACC, anterior cingulate cortex; PCC, posterior cingulate cortex; STG, superior temporal gyrus; MTG, middle temporal gyrus; Occ, Occipital cortex.

https://doi.org/10.3349/ymj.2023.0308

cortical atrophy only correlated to tau burden (Fig. 5C). Meanwhile, there were also regions in which amyloid and tau did not reveal any significant correlation: regions in which the cortical thickness was negatively correlated to amyloid and tau respectively, but the two proteinopathies were independent (Fig. 5D); regions in which the CTh was negatively correlated to tau, but positively correlated to amyloid (Fig. 5E); and regions in which the cortical atrophy correlated only to tau, without interaction with amyloid (Fig. 5F).

DISCUSSION

The present study evaluated the differential topographic distribution and correlations of tau retention and amyloid retention or cortical atrophy according to the age of onset by utilizing both amyloid and tau PET, providing five major findings. Overall, our findings showed that both amyloid and tau may play an important role in the AD pathology, but the local and non-local synergistic interaction between the two are distinct according to the age of onset, implying distinct pathogenesis between EOAD and LOAD.

In our study, LOAD patients presented a higher tau retention ratio predominantly in the medial/lateral temporal and parietal lobes. Even when compared to EOAD, the basal forebrain and the medial temporal lobe established higher tau deposition (Fig. 1), indicating that these regions are the core pathological hallmarks of LOAD. These findings may reconcile the hypothetical model proposed in the previous post-mortem studies stressing that the earliest pathological changes in LOAD tend to take place within the nerve cells of brainstem nuclei[21] and that the long projection neurons sprouting out from these regions serve as the major source of cortical and hippocampal neurotransmitters and their degeneration.[22]

It is well-known that EOAD patients display broad neuropathological changes in the overall cortices. However, few studies have compared in vivo measures of pathology or structural changes between EOAD and LOAD.[12,13] Postmortem pathologic studies have reported greater burden of amyloid-beta plaques and NFTs in the parietofrontal association cortices of EOAD patients than that in LOAD patients.[23] In concordance with previous reports, EOAD patients in our study exhibited widespread tau pathology which was only restricted to regions with tau pathologies observed in LOAD but also involved the regions beyond (e.g., occipital lobe, frontal lobe, and anterior cingulate cortex). When directly compared with LOAD, EOAD patients exhibited higher tau burden in the precuneus-PCC, inferior parietal lobule, and dorsolateral prefrontal cortex, encompassing hub regions not only in the default mode network (DMN) but also beyond the DMN, including the dorsal attention network, or in the fronto-parietal connectivity.[24-26]

Regardless of the age of onset, AD patients revealed significant local amyloid-tau correlation in the precuneus and parieto-temporal regions in common. This marked similarity in the spatial distribution of synergistic amyloid-tau interaction between EOAD and LOAD suggests the existence of neuropathological hallmarks that encompass AD spectrum regardless of the age of onset. A growing body of evidence has also highlighted the precuneus and parieto-temporal regions as the characteristic hallmark regions in AD in addition to the medial temporal lobe.[2,27-29] According to the network-based neurodegeneration theory, AD tends to target the large-scale brain network and spread along the structural or functional connectivity.[30] Among various network failures observed in AD, the disruption in the DMN has been consistently reported, and precuneus and lateral parietal cortex that have been considered as a main hub regions comprising the DMN.[30] Our findings may suggest that disruption of DMN in AD may be driven by the synergistic interaction between amyloid and tau by involving the hub regions of DMN. Despite the well-known heterogeneity of AD according to the age of onset,[1,2,28,29] the colocalization of amyloid and tau with significant local correlation preferentially observed in the precuneus and parieto-temporal regions may serve as a common neuropathological hallmark that unites EOAD and LOAD under the same eponym as AD.

However, given the inherent limitation of the cross-sectional studies, the convergent finding across the two phenotypes observed does not necessarily imply that the underlying pathomechanism is the same. Indeed, EOAD and LOAD might have gone through the same pathological course, but alternatively, they could have taken different pathways but end up developing similar spatial distribution of local amyloid-tau correlation at this stage of disease. In this regard, we would like to point out several findings that suggest a divergent pathway. First, the extent of pathological burden was much greater in EOAD both in terms of amyloid and tau. It has been consistently reported that the precuneus and parieto-temporal atrophy is more prominent in patients with a younger onset age.[1,2,29] While LOAD pathological changes progress along a stepwise pattern that initially occurs in the medial temporal lobe and later spreads to association cortices,[6] EOAD tends to show neuropathological changes earliest in the precuneus and parieto-temporal regions and then extend to other neocortical regions and also to medial temporal regions.[12] Consistent with this concept, we observed that precuneus and parieto-temporal atrophy has not yet taken place in LOAD. Taken together, although both EOAD and LOAD harbor higher amyloid and tau burden with synergistic interaction in the precuneus and parieto-temporal region, the direction of pathological spreading appears to be divergent. Second, the territory of regions exhibiting significant positive correlation between amyloid and tau burden was much wider in LOAD compared to EOAD. This difference in pathomechanism may be related to different treatment effects between the two AD subtypes depending on which pathology is targeted. A recent study showed that monoclonal antibody therapy targeting Aβ was more effective for LOAD than EAOD.[31]

Interestingly, patients with LOAD showed extensive non-local association between amyloid and tau in ROI-to-ROI correlation analyses (Fig. 5G). For example, tau deposition in the fusiform and the lateral temporal lobe showed significant correlation to amyloid deposition in widespread cortical regions, including cingulate, frontal, and parieto-occipital regions. Considering that the fusiform and lateral temporal lobe is the region to show pathological changes sequentially after the medial temporal lobe,[6] this finding can be interpreted as cortical amyloid accelerating NFTs adjacent to medial temporal lobe structures to spread out and involve the widespread neocortex.[32]

In addition to the temporal lobe, tau deposition in both lateral and medial parietal regions (i.e., precuneus) also revealed significant correlation to widespread cortical amyloid. This finding may provide a clue as to why the reduction in DMN connectivity are consistently observed in LOAD.[25,26] The parietal lobe, the core region comprising DMN, is known to be especially vulnerable to AD pathology as it faces higher metabolic demand and oxidative stress but at the same time exhibits thinner myelin sheath, thus making it more vulnerable to neuropathological burden.[2,27] However, the underlying mechanisms responsible for how amyloid and tau affect these regions has not yet been fully elucidated until now. Our study provides evidence that the parietal lobe builds up tau pathology and is correlated to distant cortical amyloid, implying that amyloid and tau interacts synergistically through brain circuits and that tau accumulation is potentially affected by cortical amyloid accumulation in LOAD.[33] Although whether amyloid truly acts as an accelerator of tauopathy in remote regions require further pathological investigations, our current study suggests that amyloid and tau may interact in a non-overlapping but a synergistic manner in the early stage of LOAD.

In contrast, the scenario appears to be different in EOAD. Unlike LOAD, EOAD patients did not show significant non-local correlation between tau and amyloid among remote regions, and even the local tau-amyloid correlation turned out to be weak except for the parietal, precuneus, and lateral temporal regions. In this regard, we postulate that tau and amyloid do not interact synergistically along neuron-to-neuron connections in the case of EOAD, but rather seem to act independently. This was contrary to our expectations, as we surmised that amyloid-tau interaction in EOAD would be extensive throughout the entire brain considering that the degree of neurodegeneration is known to be much severe in EOAD.[3,12,13] Several explanations could be applied to this finding. First, the dose effect of pathological burden could be one possible explanation. Considering that the absolute extent of pathological burden is much heavier in EOAD patients,[12,13] excessive tau and amyloid burden may independently cause cortical atrophy, even without remote accelerating effect of amyloid on tau accumulation.[10] Second, neurodegeneration in EOAD may be driven primarily by tau. Although it has long been postulated that excessive amyloid burden may be the key player of pathogenesis in EOAD, more recent data suggests that EOAD is not directly driven by amyloid deposition.[34-36] In line with these studies, region-to-region amyloid correlation of EOAD turned out to be much weaker compared to LOAD in the present study. In addition, the non-local tau-amyloid correlation was also shown to be much weaker, implying that amyloid and tau may be independent of each other not only proximity-wise but also along long-range connections in EOAD. However, in the case of tau, close links between remote regions throughout the whole neocortical regions suggest that EOAD may be driven predominantly by tau, and the propagation of tauopathy along extensive neuronal connections may account for severe, widespread neocortical atrophy.[37]

Collectively, AD appears to follow divergent pathological pathway according to the age of onset, especially in terms of molecular synergy between amyloid and tau, resulting in distinct regional neuronal vulnerability. We speculate that the neurodegeneration in EOAD, at least in this stage, may be derived by the sum of independent effects of amyloid and tau, rather than by working synergistically along neuronal connection. Alternatively, widespread neocortical atrophy of EOAD may be driven primarily by extensive tau pathology, with amyloid exerting limited local effect on limited regions, including precuneus and occipitoparietal regions.[34-36] By contrast, LOAD was characterized by extensive non-local amyloid-tau correlation between remote regions (Fig. 2 and Supplementary Fig. 3, only online).

In exploring the interplay of amyloid and tau pathology with cortical atrophy in AD, we aimed to discern whether these pathologies result from independent processes or synergistic interactions, particularly considering the differences in age of onset. In EOAD, CTh negatively correlated with regional [^{18}F]THK5351 SUVR across most cortical regions, excluding specific gyri. Commonly, CTh was negatively correlated with both [^{18}F]THK5351 and [^{18}F]FLUTE retention, with significant correlations observed in certain regions. Conversely, cortical atrophy in EOAD was primarily correlated with [^{18}F]THK5351 SUVR.

In LOAD, the regions displaying cortical atrophy associated with local [^{18}F]THK5351 SUVR were mainly situated in the temporal lobe and hippocampus. Additionally, the CTh in the orbitofrontal cortex was negatively correlated with local [^{18}F]THK5351 SUVR. While the precuneus and parieto-occipital regions in LOAD exhibited high [^{18}F]THK5351 and significant amyloid-tau correlation, neurodegeneration was not evident, leading to a lack of correlation between atrophy and amyloid or tau burden. In the entorhinal cortex, CTh was negatively correlated with local [^{18}F]THK5351 SUVR but positively correlated with [^{18}F]FLUTE SUVR, regardless of the age of onset.

For EOAD, distinct patterns of correlation emerged. Regions with mutual local correlation between amyloid and tau, such as the middle frontal gyrus, orbitofrontal cortex, precuneus, and parieto-occipital regions, suggested synergistic interactions driving regional neurodegeneration. However, in some regions such as the middle frontal gyrus and orbitofrontal cortex, corti-

https://doi.org/10.3349/ymj.2023.0308

cal atrophy was linked to both amyloid and tau independently. Regions unaffected by amyloid but influenced by tauopathy included the superior frontal gyrus, PCC, and most regions in the medial and lateral temporal lobe, indicating independent roles of amyloid and tau.

While acknowledging the concept of transneuronal interaction in EOAD, we proposed that extensive neocortical neurodegeneration might result from systemic network failures across the entire brain. Contrary to expectations, amyloid-induced tauopathy along neuronal projections might not be the primary driver of network failure in this stage of EOAD. In LOAD, significant cortical atrophy was limited to the medial and lateral temporal lobe, linked tightly to tauopathy, with amyloid indirectly contributing to neurodegeneration. The widespread territory with high tau burden exceeded the region of cortical atrophy; and beyond the temporal lobe, no association between atrophy and abnormal proteinopathies was observed. This suggests a dynamic interaction between amyloid and tau preceding neurodegeneration, particularly in regions beyond the temporal lobe, outlining a future atrophic region in LOAD.

In EOAD, elevated tau levels in the precuneus and parietal lobe correlated significantly with overall cognitive decline, impacting attention, language, and frontal executive functions. The prefrontal, PCC, lateral temporal lobe, precuneus, and parietal lobe exhibited heightened [^{18}F]THK5351 uptake, closely linked to dysfunction in visuospatial functions and memory. Even mild associations with tau burden in the medial temporal lobe were observed in memory function. EOAD, driven primarily by tauopathy, often lacks other comorbid pathologies observed in older patients, contributing to these associations. Conversely, LOAD displayed associations primarily with language and visuospatial dysfunction. Unlike EOAD, early stages of LOAD are characterized by memory-predominant dysfunction, expanding to other domains in advanced stages. No region-specific relationships were found between [^{18}F]THK5351 uptake and attention, language, or frontal executive function in LOAD, possibly due to cognitive profiles or discordance between tau deposition and cortical atrophy. The weak correlation between tau burden and cognitive dysfunction in LOAD might result from temporal delays between tau deposition and neurodegeneration, as demonstrated in this study. Unexpectedly, LOAD patients showed no significant regional associations between tau burden and delayed recall test scores in verbal and visuospatial memory. Possible explanations include the complex nature of memory retrieval, involvement of multiple cognitive domains, and the impact of comorbid pathologies, such as vascular damage or TDP-43. LOAD's complex etiology, involving interactions between amyloid and tau, suggests that tau burden alone may not fully capture cognitive dysfunction in older patients affected by multiple factors.

We note several drawbacks in our study design. First, our findings may have been affected by off-target binding. [^{18}F]THK5351 tends to show affinity for quinolone derivatives (e.g., MAO-B).[6] Considering the presence of high concentrations of MAO-B in the cerebral cortex and basal ganglia, the interpretation of [^{18}F]THK5351 PET images may be confounded due to MAO-B affinity. Recent studies have shown that the majority of THK5351 signal is due to binding to MAO-B rather than tau deposition.[14-16] Although THK distinguished AD patients from controls, this discrimination could be based on neuroinflammation. Therefore, it would be difficult to assert that THK5351 retention reflects tau deposition. Second, our study cannot fully address the temporal sequence or causal relationships between amyloid, tau, and cortical atrophy due to the inherent limitation of the cross-sectional study design. Third, we adopted the conventional cut-off point, the age of 65 years, in determining EOAD and LOAD. Although there has been a general agreement that a 65 year cut-off serves as an efficient determinant of EOAD, this cut-off is an arbitrary division based on sociological aspects and is not strongly supported by biological evidence.[38] In this regard, it may be inadequate to dichotomize EOAD and LOAD solely on the basis of age of onset alone. Therefore, multiple factors, such as clinical symptoms, genotype, neurodegenerative patterns, and burden, should be incorporated to define EOAD and LOAD in a more scientific manner.

Despite the limitations, our present work still holds several strengths. First, all participants underwent both amyloid and tau PET imaging along with structural MRI scans in our prospective study. By doing so, we could tease out several representative patterns of relationship among amyloid and tau deposit, and brain tissue loss. The differential relationships according to the age of onset captured in our study shed light on the potential mechanism of EOAD and LOAD pathogenesis. Second, we investigated not only the differential distribution of amyloid and tau, but also the local and non-local amyloid-tau correlations, and thereby showed that these two proteinopathies might interact both locally and at a large scale. A recent clinical study showed ananti-amyloid therapy was more effective on the patients with LOAD rather than patients with EOAD.[31] The different correlation between amyloid and tau might result in different effects of disease-modifying therapy. This study may have implications for future disease-modifying therapeutic trials targeting amyloid or tau pathologies.

ACKNOWLEDGEMENTS

We would like to thank Professor Kwang-Woo Lee for sharing the idea for this study. This study was supported by a grant from the Korea Healthcare Technology R&D Project through the Korea Health Industry Development Institute (KHIDI), funded by the Ministry of Health & Welfare of the Republic of Korea (grant number: HI14C1135), a grant from the Basic Science Research Program through the National Research Foundation of Korea (NRF), funded by the Ministry of Education (grant number: 2021R1A6A1A03038996), and a grant from Gachon University Gil Medical Center (grant number: FRD2022-16).

AUTHOR CONTRIBUTIONS

Conceptualization: Han Kyu Na, Joon-Kyung Seong, and Young Noh. Data curation: Han Kyu Na, Seongho Seo, Woo-Ram Kim, Justin Byun, and Young Noh. Formal analysis: Jeong-Hyeon Shin, Seongho Seo, Jaelim Cho, and Joon-Kyung Seong. Funding acquisition: Young Noh. Investigation: Seongho Seo, Woo-Ram Kim, Sang-Yoon Lee, and Jaelim Cho. Methodology: Jeong-Hyeon Shin, Sung-Woo Kim, Seongho Seo, and Jaelim Cho. Project administration: Young Noh. Resources: Jae Myeong Kang, Sang-Yoon Lee, Nobuyuki Okamura, and Young Noh. Software: Jeong-Hyeon Shin, Sung-Woo Kim, and Seongho Seo. Supervision: Nobuyuki Okamura, Joon-Kyung Seong, and Young Noh. Validation: Seongho Seo, Woo-Ram Kim, and Joon-Kyung Seong. Visualization: Jeong-Hyeon Shin, Seongho Seo, and Woo-Ram Kim. Writing—original draft: Han Kyu Na and Jeong-Hyeon Shin. Writing—review & editing: Joon-Kyung Seong and Young Noh. Approval of final manuscript: all authors.

ORCID iDs

Han Kyu Na	https://orcid.org/0000-0002-2093-1641
Jeong-Hyeon Shin	https://orcid.org/0000-0002-8680-256X
Sung-Woo Kim	https://orcid.org/0009-0006-0558-1635
Seongho Seo	https://orcid.org/0000-0001-7894-0535
Woo-Ram Kim	https://orcid.org/0000-0003-1361-4426
Jae Myeong Kang	https://orcid.org/0000-0003-0803-9332
Sang-Yoon Lee	https://orcid.org/0000-0002-6029-8553
Jaelim Cho	https://orcid.org/0000-0002-4524-0310
Justin Byun	https://orcid.org/0000-0002-7953-8238
Nobuyuki Okamura	https://orcid.org/0000-0002-5991-7812
Joon-Kyung Seong	https://orcid.org/0000-0001-8227-5849
Young Noh	https://orcid.org/0000-0002-9633-3314

REFERENCES

1. Murray ME, Graff-Radford NR, Ross OA, Petersen RC, Duara R, Dickson DW. Neuropathologically defined subtypes of Alzheimer's disease with distinct clinical characteristics: a retrospective study. Lancet Neurol 2011;10:785-96.
2. Na HK, Kang DR, Kim S, Seo SW, Heilman KM, Noh Y, et al. Malignant progression in parietal-dominant atrophy subtype of Alzheimer's disease occurs independent of onset age. Neurobiol Aging 2016;47:149-56.
3. Frisoni GB, Pievani M, Testa C, Sabattoli F, Bresciani L, Bonetti M, et al. The topography of grey matter involvement in early and late onset Alzheimer's disease. Brain 2007;130(Pt 3):720-30.
4. Sá F, Pinto P, Cunha C, Lemos R, Letra L, Simões M, et al. Differences between early and late-onset Alzheimer's disease in neuropsychological tests. Front Neurol 2012;3:81.
5. Marshall GA, Fairbanks LA, Tekin S, Vinters HV, Cummings JL. Early-onset Alzheimer's disease is associated with greater pathologic burden. J Geriatr Psychiatry Neurol 2007;20:29-33.
6. Harada R, Okamura N, Furumoto S, Furukawa K, Ishiki A, Tomita N, et al. 18F-THK5351: a novel PET radiotracer for imaging neurofibrillary pathology in Alzheimer disease. J Nucl Med 2016;57:208-14.
7. Villemagne VL, Furumoto S, Fodero-Tavoletti MT, Mulligan RS, Hodges J, Harada R, et al. In vivo evaluation of a novel tau imaging tracer for Alzheimer's disease. Eur J Nucl Med Mol Imaging 2014;41:816-26.
8. Cho H, Choi JY, Hwang MS, Kim YJ, Lee HM, Lee HS, et al. In vivo cortical spreading pattern of tau and amyloid in the Alzheimer disease spectrum. Ann Neurol 2016;80:247-58.
9. Sepulcre J, Schultz AP, Sabuncu M, Gomez-Isla T, Chhatwal J, Becker A, et al. In vivo tau, amyloid, and gray matter profiles in the aging brain. J Neurosci 2016;36:7364-74.
10. Pimplikar SW, Nixon RA, Robakis NK, Shen J, Tsai LH. Amyloid-independent mechanisms in Alzheimer's disease pathogenesis. J Neurosci 2010;30:14946-54.
11. Pascoal TA, Mathotaarachchi S, Mohades S, Benedet AL, Chung CO, Shin M, et al. Amyloid-β and hyperphosphorylated tau synergy drives metabolic decline in preclinical Alzheimer's disease. Mol Psychiatry 2017;22:306-11.
12. Cho H, Choi JY, Lee SH, Lee JH, Choi YC, Ryu YH, et al. Excessive tau accumulation in the parieto-occipital cortex characterizes early-onset Alzheimer's disease. Neurobiol Aging 2017;53:103-11.
13. Schöll M, Ossenkoppele R, Strandberg O, Palmqvist S, Jögi J, Ohlsson T, et al. Distinct 18F-AV-1451 tau PET retention patterns in early- and late-onset Alzheimer's disease. Brain 2017;140:2286-94.
14. Harada R, Ishiki A, Kai H, Sato N, Furukawa K, Furumoto S, et al. Correlations of 18F-THK5351 PET with postmortem burden of tau and astrogliosis in Alzheimer disease. J Nucl Med 2018;59:671-4.
15. Lee HJ, Lee EC, Seo S, Ko KP, Kang JM, Kim WR, et al. Identification of heterogeneous subtypes of mild cognitive impairment using cluster analyses based on PET imaging of tau and astrogliosis. Front Aging Neurosci 2021;12:615467.
16. Harada R, Furumoto S, Kudo Y, Yanai K, Villemagne VL, Okamura N. Imaging of reactive astrogliosis by positron emission tomography. Front Neurosci 2022;16:807435.
17. Cho Y, Seong JK, Jeong Y, Shin SY; Alzheimer's Disease Neuroimaging Initiative. Individual subject classification for Alzheimer's disease based on incremental learning using a spatial frequency representation of cortical thickness data. Neuroimage 2012;59:2217-30.
18. Greve DN, Salat DH, Bowen SL, Izquierdo-Garcia D, Schultz AP, Catana C, et al. Different partial volume correction methods lead to different conclusions: an (18)F-FDG-PET study of aging. Neuroimage 2016;132:334-43.
19. Greve DN, Svarer C, Fisher PM, Feng L, Hansen AE, Baare W, et al. Cortical surface-based analysis reduces bias and variance in kinetic modeling of brain PET data. Neuroimage 2014;92:225-36.
20. Thurfjell L, Lilja J, Lundqvist R, Buckley C, Smith A, Vandenberghe R, et al. Automated quantification of 18F-flutemetamol PET activity for categorizing scans as negative or positive for brain amyloid: concordance with visual image reads. J Nucl Med 2014;55:1623-8.
21. Braak H, Del Tredici K. The preclinical phase of the pathological process underlying sporadic Alzheimer's disease. Brain 2015;138(Pt 10):2814-33.
22. Schliebs R, Arendt T. The cholinergic system in aging and neuronal degeneration. Behav Brain Res 2011;221:555-63.
23. Hansen LA, DeTeresa R, Davies P, Terry RD. Neocortical morphometry, lesion counts, and choline acetyltransferase levels in the age spectrum of Alzheimer's disease. Neurology 1988;38:48-54.
24. Adriaanse SM, Binnewijzend MA, Ossenkoppele R, Tijms BM, van der Flier WM, Koene T, et al. Widespread disruption of functional brain organization in early-onset Alzheimer's disease. PLoS One 2014;9:e102995.
25. Gour N, Felician O, Didic M, Koric L, Gueriot C, Chanoine V, et al. Functional connectivity changes differ in early and late-onset Alzheimer's disease. Hum Brain Mapp 2014;35:2978-94.
26. Vincent JL, Kahn I, Snyder AZ, Raichle ME, Buckner RL. Evidence for a frontoparietal control system revealed by intrinsic functional connectivity. J Neurophysiol 2008;100:3328-42.
27. Bruner E, Jacobs HI. Alzheimer's disease: the downside of a highly evolved parietal lobe? J Alzheimers Dis 2013;35:227-40.

https://doi.org/10.3349/ymj.2023.0308

28. Park JY, Na HK, Kim S, Kim H, Kim HJ, Seo SW, et al. Robust identification of Alzheimer's disease subtypes based on cortical atrophy patterns. Sci Rep 2017;7:43270.
29. Noh Y, Jeon S, Lee JM, Seo SW, Kim GH, Cho H, et al. Anatomical heterogeneity of Alzheimer disease: based on cortical thickness on MRIs. Neurology 2014;83:1936-44.
30. Buckner RL, Sepulcre J, Talukdar T, Krienen FM, Liu H, Hedden T, et al. Cortical hubs revealed by intrinsic functional connectivity: mapping, assessment of stability, and relation to Alzheimer's disease. J Neurosci 2009;29:1860-73.
31. van Dyck CH, Swanson CJ, Aisen P, Bateman RJ, Chen C, Gee M, et al. Lecanemab in early Alzheimer's disease. N Engl J Med 2023;88:9-21.
32. Mattsson N, Insel PS, Nosheny R, Tosun D, Trojanowski JQ, Shaw LM, et al. Emerging β-amyloid pathology and accelerated cortical atrophy. JAMA Neurol 2014;71:725-34.
33. Iaccarino L, Tammewar G, Ayakta N, Baker SL, Bejanin A, Boxer AL, et al. Local and distant relationships between amyloid, tau and neurodegeneration in Alzheimer's disease. Neuroimage Clin 2017;17:452-64.
34. Panegyres PK, Chen HY. Differences between early and late onset Alzheimer's disease. Am J Neurodegener Dis 2013;2:300-6.
35. Rabinovici GD, Furst AJ, Alkalay A, Racine CA, O'Neil JP, Janabi M, et al. Increased metabolic vulnerability in early-onset Alzheimer's disease is not related to amyloid burden. Brain 2010;133(Pt 2):512-28.
36. Morris GP, Clark IA, Vissel B. Inconsistencies and controversies surrounding the amyloid hypothesis of Alzheimer's disease. Acta Neuropathol Commun 2014;2:135.
37. Wu JW, Hussaini SA, Bastille IM, Rodriguez GA, Mrejeru A, Rilett K, et al. Neuronal activity enhances tau propagation and tau pathology in vivo. Nat Neurosci 2016;19:1085-92.
38. Masellis M, Sherborn K, Neto P, Sadovnick DA, Hsiung GY, Black SE, et al. Early-onset dementias: diagnostic and etiological considerations. Alzheimers Res Ther 2013;5(Suppl 1):S7.